Journal of Biomedical Optics 5(3), 291–299 (July 2000)

Theoretical foundations for noninvasive measurement of variations in the width of the subarachnoid space

Jerzy Pluciński
Technical University of Gdańsk
Department of Optoelectronics
Faculty of Electronics, Telecommunications and Informatics
Ul. Narutowicza 11/12, 80-952 Gdańsk, Poland

Andrzej F. Frydrychowski
Jacek Kaczmarek
Witold Juzwa
Medical University of Gdańsk
Department of Physiology
PL-80-211 Gdańsk, Poland

Abstract. Numerical modeling was used for the theoretical analysis of the propagation of optical radiation in the tissues of the human head, generated by a single source placed on the surface of the scalp. Of special interest and importance is the propagation of radiation within the layer of cerebrospinal fluid contained in the subarachnoid space (SAS), which is the only low absorption/high transmittance medium whose width can vary rapidly. Qualitative and quantitative assessment of changes in propagation of radiation within the SAS could become a source of information on changes in the geometry of this anatomical compartment playing a crucial role in cranio-spinal physiology and pathology. Essential for the idea of the possible noninvasive assessment of changes in width of the SAS by an optical method is the dependence of intensity of radiation reaching a photodetector located at a certain distance from the source on changes in the width of this fluid layer, which acts like a biological optical waveguide. Monte Carlo modeling and numerical analysis confirmed the feasibility of assessing changes in the width of the subarachnoid space optically. Presented here are details of the Monte Carlo simulation of light propagation in the tissues of human head and the results of such simulation as a function of the width of the subarachnoid space, calculated for different distances between the source and detector and for a few selected values of bone thickness. Results of numerical modeling were then compared with those of experiments on a mechanical-optical model. © *2000 Society of Photo-Optical Instrumentation Engineers.* [S1083-3668(00)01103-5]

Keywords: optical radiation; propagation in tissues of the head; numerical modeling; optical measurement; subarachnoid space.

Paper JBO-NIT-001 received May 29, 1998; revised manuscript received June 11, 1999 and Jan. 27, 2000; accepted for publication Feb. 7, 2000.

1 Introduction

Noninvasive methods of assessment of physiological processes as well as of changes in structure and function of the human body in cases of pathology continue to be among the most important objectives of intensive research carried out by scientists of various disciplines. One of the very promising techniques, whose successful application may provide much information on intracranial homeostasis, including changes in brain volume and cerebrovascular pulsation, appears to be transillumination or—when the light source and detector are close to each other—reflectance of the head. The method involves the quantitative analysis of optical radiation penetrating the soft tissues of the head and the skull bones. Although the first experiments with transillumination of the head were described by Kreutermann as early as in the 18th century, and by Bright in the first half of the 19th century,[1] the method has not been fully developed due to the complex nature of the phenomena involved in light propagation in the structures of the human head as well as due to a lack of appropriate measuring and data-processing equipment in the pre-electronic era.

In adults, light transillumination or diffuse reflectance was not recognized as valuable mainly due to the very low transparency to visible (white) light of adult human skull bones resulting from the bone thickness, and the related serious difficulties in interpretation. In infants, attempts were made to employ visible light for assessment of magnitude of hydrocephalus.[2]

Contemporary medical diagnostic techniques utilizing optical radiation are mostly based on spectroscopy. Measurement of absorbance of radiation of given wavelengths by hemoglobin and other chromophores variably saturated with oxygen, serves mainly the purpose of oximetry, i.e., measurement of oxygen supply to the examined tissue or organ. This method has proved valuable also in the assessment of oxygen supply to the brain. This technique employs mainly near-infrared radiation (NIR).[3–5]

Address all correspondence to Jerzy Pluciński. Tel: +48 58 3472642; Fax: +48 58 3471848; E-mail: pluc@pg.gda.pl

1083-3668/2000/$15.00 © 2000 SPIE

Before the stream of optical radiation reaches the target tissue of the brain, it undergoes significant dissipation and absorption in the skull bones. Initially, this posed a major limitation for the application of this method in adults, whose skull bones are relatively thick and constitute a serious obstacle to the propagation of radiation. However, with time and technological progress, diagnostic techniques utilizing NIR have become valuable tools in oximetric examination of the brain not only in infants but also in adult patients.[6–18]

As optical radiation appears to remain the most suitable information-bearing signal for noninvasive assessment of changes in cerebral hemodynamics and width of the subarachnoid space (SAS)—reflecting changes in the volume of the brain—the method of NIR transillumination fully deserves further extensive research.

In the transillumination of the head the objects of examination with optical radiation are the anatomical structures of the head, such as skin, skull bones, cerebrospinal fluid (CSF) in the SAS and the brain tissue. While penetrating these different optical media, photons are subject to absorption, scattering in various directions—including forward and retrograde propagation directions, as well as reflection at the boundaries of neighboring optical media, e.g., CSF layer in SAS/surface of the brain.

A better understanding of the phenomena governing propagation of optical radiation in layers of various human tissues could allow for the elaboration and application in medical practice of techniques that utilize optical radiation as the information-bearing medium. Introduction of such noninvasive techniques would be of unmatched importance for assessment of changes in intracranial homeostasis and particularly fluid space volume reserve and cerebrovascular pulsation.

The objective of this study is to explore with numerical modeling the feasibility of assessing changes in the width of the SAS with a noninvasive optical method. Strictly speaking, numerical modeling is expected to reveal the pathway for best propagation of optical radiation and the relations between the propagation magnitude and thickness of particular tissue layers. We think the results of numerical modeling should also provide us with some useful hints for designing new sensors and measuring devices. With the assumption that the source and detector of optical radiation are both placed on the surface of the head, numerical modeling should answer the following questions: (1) What is the maximum source-detector distance at which the power of radiation reaching the detector is sufficient to be measured by available optoelectronic equipment? (2) How does the propagation of radiation change with changes in the width of the SAS? (3) How far from the source should the detector be located to assure optimum sensitivity to such alterations? Moreover, numerical modeling is expected to enable analysis of the conditions under which the detector receives a stream of radiation composed mainly of photons which are propagated via the superficial path in the scalp and bone, i.e., are not propagated via the paths through deeper lying tissues. The additional monitoring of simultaneous measurement of transmission of radiation via the superficial path could then allow for the extraction from the measured transmission, of a signal dependent exclusively on the rhythmic changes in the width of the SAS, with elimination of its modulations resulting from the pulsation of superficial arteries of the scalp. The frequency of these fluctuations is equal to the heart rate (HR).

2 Method of Analysis

2.1 Analysis of Propagation of Optical Radiation in Human Tissues

Human tissues are characterized by a high complexity of structure, which is the reason why it is rather difficult to describe the propagation of optical radiation in media of this kind. Propagation of radiation in tissue depends both on the absorption in the tissue and on the scattering. For transmission of very short ultraviolet and infrared radiation, tissue absorption may be substantially greater than scatter.

The length of photon path from scatter to scatter is a random variable, whose probability density function is

$$p_s(r_s)=\mu_s \exp(-\mu_s r_s), \tag{1}$$

where r_s is a length of photon path, μ_s is the scattering coefficient.

The deflection of a photon once it is scattered is specified by a phase function $p(\mathbf{s}',\mathbf{s})$, which describes the probability of a photon to be scattered from a direction $\mathbf{s}$ to a direction $\mathbf{s}'$. Since the phase function is the only parameter which can be measured independently using thin slices and goniometric equipment, several functions have been discussed in the literature to enable the best fit to experimental data (isotropic, Henyey–Greenstein, Delta–Eddington, Rayleigh–Gans, etc.).[19–23] The authors used the Henyey–Greenstein phase function

$$p_{\cos\theta}(\cos\theta)=\frac{1}{2}\frac{1-g^2}{(1+g^2-2g\cos\theta)^{3/2}}$$

or (2)

$$p_\theta(\theta)=\frac{\sin\theta}{2}\frac{1-g^2}{(1+g^2-2g\cos\theta)^{3/2}},$$

where $\underline{\theta}$ is a scattering angle, such that

$$\int_{-1}^{1} p_{\cos\theta}(\cos\theta)d(\cos\theta)=1 \quad \text{or} \quad \int_0^{\pi} p_\theta(\theta)d\theta=1 \tag{3}$$

and g is an anisotropy factor fulfilling the following condition:

$$g=\int_{-1}^{1} p_{\cos\theta}(\cos\theta)\cos\theta d(\cos\theta)=\langle\cos\theta\rangle$$

or (4)

$$g=\int_0^{\pi} p_\theta(\theta)\cos\theta d\theta=\langle\cos\theta\rangle,$$

where $\langle\cdot\rangle$ stands for the average value. The anisotropy factor can vary from -1 up to 1.

In an absorptive medium photons undergo absorption. The length of path followed by a photon before its absorption is a random variable, whose probability density function is

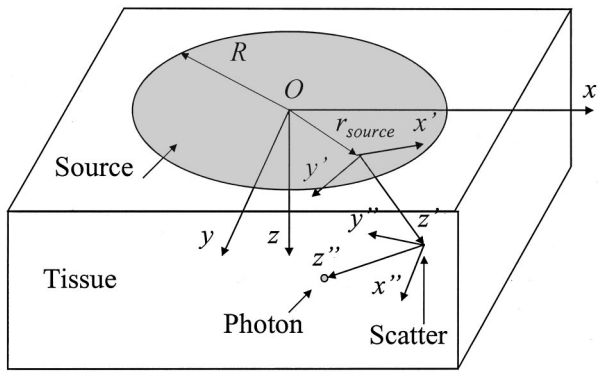

Fig. 1 Schematic diagram of the optical source, photon paths in the tissue and system coordinates.

$$p_a(r_a)=\mu_a \exp(-\mu_a r_a), \tag{5}$$

where r_a is a length of photon path, μ_a is the absorption coefficient.

For a highly scattering medium, we may consider the system to be isotropic, and the propagation of the photons can be described using the Boltzman transport equation[24]

$$\frac{1}{v}\frac{\partial L(\mathbf{r},\mathbf{s},t)}{\partial t}=-\mathbf{s}\cdot\nabla L(\mathbf{r},\mathbf{s},t)-\mu_a L(\mathbf{r},\mathbf{s},t)-\mu_s L(\mathbf{r},\mathbf{s},t)$$
$$+\mu_s\int_{4\pi}p(\mathbf{s}',\mathbf{s})L(\mathbf{r},\mathbf{s}',t)d\Omega'+\epsilon(\mathbf{r},\mathbf{s},t), \tag{6}$$

where v is the velocity of optical radiation in the medium ($v=c/n$, c is the velocity of optical radiation in vacuum, n is the refractive index of the medium), Ω' is spatial angle, $L(\mathbf{r},\mathbf{s},t)$ is the photon flux at position $\mathbf{r}$ and time t, and $\epsilon(\mathbf{r},\mathbf{s},t)$ represents the source of radiation.

While the motion cannot in general be derived analytically for any arbitrary shape medium, Eq. (6) can be used as the basis for iterative[25] or Monte Carlo calculations.[25,26] To solve Eq. (6), a special computer program was composed by one of us (J. Pluciński). This program uses the Monte Carlo method where each photon changes its weight coefficient in order with a weight function for the absorption coefficient.[27] For clarity, it should be noted that this use of the term ''photon'' has little in common with the quantum theory of optical radiation but it is a simplification used by the Monte Carlo simulation.

In this program, the source of optical radiation (Figure 1) is modeled as a disk of radius R whose radiance is modeled by a raised-cosine function and by selecting an adequate value of m

$$\epsilon(\mathbf{r},\mathbf{s},t)=\begin{cases}A_0(\cos\alpha)^m & \text{if } r_{\text{source}}\leqslant R \text{ and } r_z=0\\ 0 & \text{if } r_{\text{source}}>R \text{ or } r_z\neq 0,\end{cases} \tag{7}$$

where $r_{\text{source}}=\sqrt{r_x^2+r_y^2}$, α is the angle between $\mathbf{s}$ and z direction, r_x, r_y and r_z are vector $\mathbf{r}$ components, A_0 is the radiance in z direction.

The computer program uses a random number generator of real numbers x_{RN} in range $<0;1)$ with probability density function $p(x_{\text{RN}})=1$ by Knuth.[28,29] It is assumed that the source of photons lies on the surface $z=0$ and the $\mathbf{z}$ axis is perpendicular to the source (Figure 1). If each photon is assigned its local $\mathbf{x}'\mathbf{y}'\mathbf{z}'\mathbf{O}$ coordinate system in which it propagates along $\mathbf{z}'$ axis, the Euler angles relating this system to the global $\mathbf{xyzO}$ coordinate system are

$$\theta=\arccos(1-(1-\cos\alpha_{\max})x_{\text{RN}})$$
$$\varphi=2\pi x_{\text{RN}}=0. \tag{8}$$

The weight coefficient of each generated photon depends on the direction of its propagation, according to Eq. (7) assuming that $A_0=1$. The power of the radiation generated by the source is calculated as a sum of weight coefficients of photons which leave the source. The power mentioned above is expressed in arbitrary units.

The input data for modeling of the tissues include their dimensions, scattering coefficient μ_s, attenuation coefficient μ_a and anisotropy factor g. The direction and position of the photon changes from scatter to scatter in a random way until the photon manages to exit from the tissues or the photon weight coefficient is smaller than a given value.

The length of path from scatter to scatter is calculated according to the density function (1)

$$r_s=\frac{-\ln(1-x_{\text{RN}})}{\mu_s}. \tag{9}$$

Every time photon scattering occurs, a new local $\mathbf{x}''\mathbf{y}''\mathbf{z}''\mathbf{O}$ coordinate system is introduced, in which the photon propagates along the $\mathbf{z}''$ axis. The $\mathbf{x}''\mathbf{y}''\mathbf{z}''\mathbf{O}$ coordinate system is related to the previous local $\mathbf{x}'\mathbf{y}'\mathbf{z}'\mathbf{O}$ coordinate system of the photon by the Euler angles

$$\theta=\arccos\left\{\frac{1}{2g}\left[1+g^2-\left(\frac{1-g^2}{1-g+2gx_{\text{RN}}}\right)^2\right]\right\},$$
$$\varphi=2\pi x_{\text{RN}}=0. \tag{10}$$

The weight coefficient is calculated from the total length of the photon path l

$$\epsilon_{\text{out}}=\epsilon_{\text{in}}e^{-\mu_a l}, \tag{11}$$

where ϵ_{in} is the weight coefficient of photon entering the tissue, ϵ_{out} is the weight coefficient of the photon leaving the tissue.

The input data for modeling of the detector are its dimensions, location and aperture angle. The power of radiation (expressed in arbitrary unit) received by the detector is calculated as a sum of weight coefficients of the photons, which reach the detector. The actual power of the received radiation can be calculated by multiplying the received/emitted power ratio, expressed in arbitrary units, and the actual power of the source. As a result, we get the surface distribution of power as a function of the detector location. These results are stored in files to generate charts with specialized software (for example, with Excel™ or Statistica™ programs).

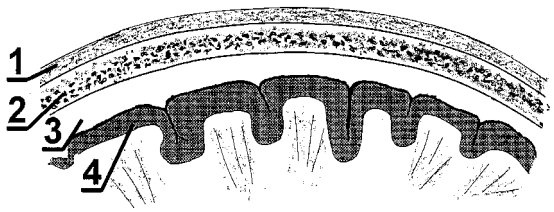

Fig. 2 Cross section of the modeled set of tissues: 1-scalp, 2-skull, 3-cerebrospinal fluid, 4-brain.

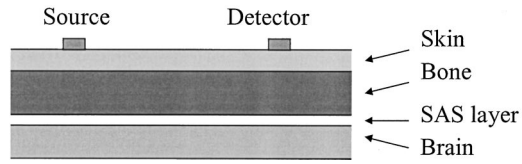

Fig. 3 Schematic diagram showing consecutive layers of tissues and the location of the source and detector against each other.

2.2 Optical Model of Tissues of the Head

The cross section of the modeled head tissues in the frontal region is presented in Figure 2.

The simplified model of the adult human head is a multilayer block 10 cm wide×10 cm high×3 cm thick. The first, outer layer 3 mm thick is the skin with the subcutaneous tissue. Below it there is the skull bone of heterogeneous structure. The bone consists of two compact laminae of 2.5 mm with porous spongy lamina containing air and fat between them. As the optical densities of the layers are not identical, two different parameters were assumed for them in the model. The thickness of the skull bones varies between individuals over the range from 3 to 15 mm, according to the results of our own measurements (see measurement experiment). More than 80% of the investigated skull bones fell within the range 3–12 mm. For the numerical modeling, four most common thicknesses of skull bones were chosen from that range (3, 6, 9, and 12 mm). Deeper below the skull bone there is another different layer, composed of the cerebrospinal fluid, which fills the SAS between the inner surface of the skull bone and the surface of the brain, surrounding the brain like a soft cushion. The thickness of this layer, i.e., width of the SAS, varies between regions of the cranial cavity in the range from 0.5 to 2 mm. The last layer is the brain tissue. The model consists of four layers, in which propagation of photons occurs, three of them characterized by significantly higher optical density (skin, bone, brain tissue) than the cerebrospinal fluid. In the light of the results of model studies by Okada et al.,[30] who found weak dependence of transmission of optical radiation on the texture of the brain surface, in our study the latter was assumed to be smooth.

For the sake of simplification of the calculations an assumption was made of isotropy of the tissues and homogeneity of their optical parameters. It was also assumed that the border surfaces between the consecutive layers are planes parallel to the skin surface (Figure 3). The **xyzO** system of coordinates was designed in such a way that the source of radiation was located in its very center (0,0,0) and the **z** axis was perpendicular to skin surface and directed towards the brain.

The modeled source of radiation was a light-emitting diode (LED)-type SFH 484-3 by Siemens. For the modeling procedure the following source parameters were assumed: aperture diameter 5 mm, directional characteristics as described in formula (7) with the m parameter equal to 70.88, which corresponds to an emission angle $\pm 8°$; the power of the source was 134 mW (impulse mode with impulse current 537 mA).

For the photodetector a photodiode-type BPW-34 by Siemens was modeled, with a photosensitive area of 7.45 mm^2.

Values of parameters used as input data for the numerical modeling are presented in Table 1.

Notes:

(a) There are major discrepancies between the values of the above parameters in the works by different authors. This is particularly true in the case of the absorption coefficient (e.g., its value can be $\mu_a = 0.013\ 1/\mathrm{mm}$[31] or $\mu_a = 0.025\ 1/\mathrm{mm}$[32] or even $\mu_a = 0.45\ 1/\mathrm{mm}$[33]). For the calculations we chose such values of the parameters which cause relatively high attenuation of the power of the signal.

(b) At distances from the source markedly exceeding $1/\mu_s$, power distribution does not depend on the scattering coefficient and scattering anisotropy coefficient if the reduced scattering coefficient μ_s' ($\mu_s' = \mu_s(1-g)$) remains constant. Therefore, for the sake of reduction of the calculation time, an isotropic model of propagation of radiation within the bones, SAS and brain was assumed in which $g=0$ and $\mu_s = \mu_s'$. An anisotropic model of propa-

Table 1 Optical properties of tissues of the head used for numerical modeling.

Tissue	Thickness [mm]	Absorption coefficient μ_a [1/mm]	Scattering coefficient μ_s [1/mm]	Anisotropy coefficient g	Reduced scattering coefficient μ_s' [1/mm]	Reference
Skin	3	0.27	18.7	0.82		34
Bone	3, 6, 9, 12	0.0269			0.86	35
SAS	0–5	0.001	0.001	0.0		
Brain	10	0.038	65.0	0.97		36

gation was assumed for the skin, to enable analysis of situation, when the photodetector is located in very close proximity to the source.

(c) In Ref. 35 parameters for the skull were given for wavelengths of 849 and 956 nm. The value for 890 nm, needed for our calculations, was obtained through approximation.

(d) The width of the fluid layer in the SAS changed in the range from 0 to 5 mm, calculations were made with increments of 0.1 mm; absorption and scatter were neglected because they are minute, compared with the bordering tissues, however, nonzero values for both absorption and scatter coefficients were assigned (0.001 l/mm and 0.001 l/mm, respectively) in order to avoid division by zero in the calculation procedure; the scatter anisotropy coefficient was assumed to be 0.

(e) The width of the fluid layer was assumed to be much greater than in real conditions (about 4 mm) and much greater than the depth of the intracerebral penetration by NIR light. The penetration depth is equal to $\sqrt{1/(3\mu_a(\mu_a+(1-g)\mu_s))}$,[37] which is much less than the thickness of the brain layer (for brain of $\mu_a = 0.038$ 1/mm, $\mu_s = 65.0$ 1/mm, $g = 0.97$ at 890 nm, the penetration depth of brain tissue equals 2.1 mm). Such an assumption eliminates the need for modeling the deeper layers of the brain in this model study. Increasing the depth of penetration in this model study led to a marked increase in model calculation time, with no change observed in the distribution of power of radiation on the surface of the head. In studies by other authors, other values of parameters for the skull can be found, e.g., in Ref. 38 $\mu_a = 0.03$ 1/mm, $\mu_s = 26.0$ 1/mm, $g = 0.94$ at 890 nm.

The distance ranges from the source in directions **x** and **y** were limited to 5 cm with a view to reduce the time needed for the calculations. The calculation time was further cut down through introduction of a minimal weight coefficient $\epsilon_{\min}$ for each photon, below which value calculations for a given photon were abandoned. The coefficient was 10^{-30}, while the weight coefficient for each photon upon its generation by the source was equal to 1 in the perpendicular direction; its values were lower than 1 for the other directions to preserve the directional characteristics of the source—see formula (7). Further reduction of calculation time was obtained by performing parallel calculations for different widths of the SAS. When a photon left the tissues without reaching the SAS, then an identical path of the photon was assumed for all widths of the SAS. Therefore, only for very few photons, namely those that reached the SAS, was it necessary to calculate individual paths within that space, and this only at the distance SAS—surface of the skin. In determining transmission as a function of the source-detector distance, the isotropy of the system was used in directions perpendicular to the ***z*** axis. Therefore, with the source of radiation characterized by axial symmetry about the ***z*** axis, we receive a planar distribution of the power of photons leaving the tissues through the skin, which also reveals axial symmetry. It was assumed then,

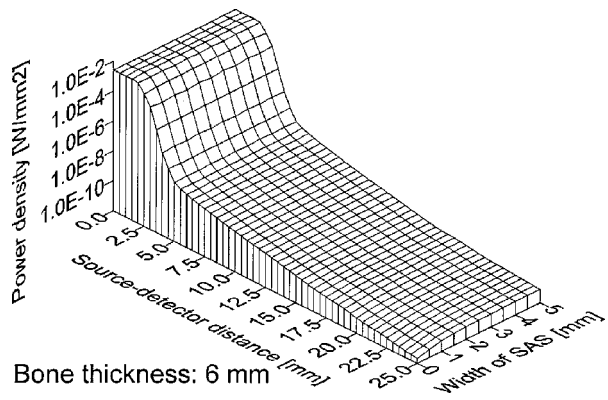

Fig. 4 Surface distribution of received power density vs distance from the source and width of SAS (100 million photons).

that the power of the radiation reaching a detector of $a \times a$ dimension, located a distance d from the source, is equal to the summed power of the photons leaving the skin in the distance interval $d \pm a/2$ from the source multiplied by the factor $a/(2\pi d)$.

3 Numerical Results

Presented below are the results of modeling of transmission of optical radiation in tissues of the human head; the number of photons analyzed was 100 million (Figure 4 and Figure 6) or 10 million (Figure 5). This number is a result of compromise between accuracy of the results and the time required for calculations.

Figure 4 shows the distribution of power density on the surface of the head as a function of the distance from the source (1 W power) and the SAS width, for a frontal bone thickness of 6 mm. For the assumed LED source of 134 mW power and for a detector active area of 7.45 mm^2, the power of radiation received by the detector can be calculated by multiplying the surface power density plotted in Figure 4 by the factor 1.

Similar relations between the distribution of power density on the surface of the head as a function of the distance but for a SAS width 1 mm and for different thickness of skull bone, are shown in Figure 5. The amount of radiation, which was propagated in the skin or in the skin and bone only, are also presented in Figure 5.

For potential constructors of a system for measurement of the width of the SAS it is very important to know the magnitude of relative changes in power of the optical radiation as a function of the width of that space for a given source-detector distance. This relation is presented in Figure 6. The distance from source was limited to 25 mm to ensure the power of radiation received was not less than 1 pW for all bone thicknesses under the conditions described above.

4 Measurement Experiment

For the future utilization of the method in clinical practice, it was necessary to identify the power level of the optical source that would have to be used, as well as the sensitivity of the detectors for skull bones of different thickness. Therefore the average thickness of skull bones was determined during au-

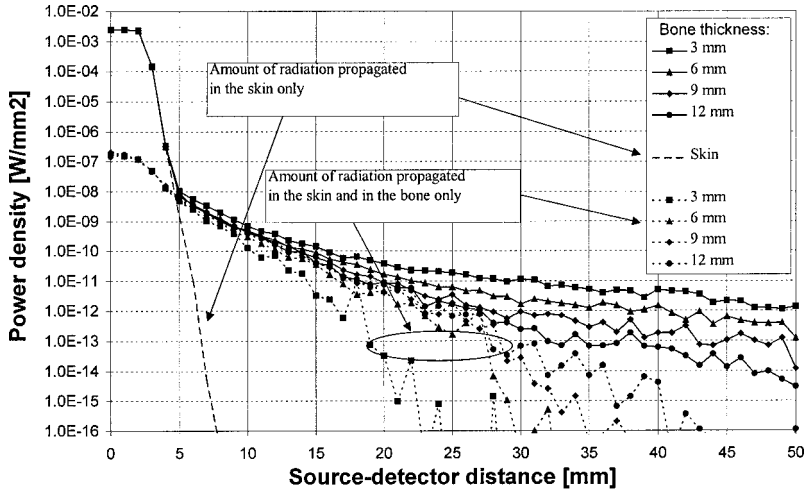

Fig. 5 Surface distribution of received power density vs source-detector distance for SAS of 1 mm width (10 million photons).

topsy in 150 cadavers of both sexes, age 18 through 83 years. Measurements were made with a micrometer. The results are presented in Figure 7.

We also examined the character of the relation between NIR transmission ratio and thickness of the skull bone. Figure 8 shows the dramatic decrease of NIR transmission ratio with increase in bone thickness. An exponential curve fitted the experimental data well and shows the character of the dependence of NIR propagation with thickness.

Experiments designed to verify the results of numerical modeling, presented in this study, were carried out on a simplified mechanical-optical model (tester) imitating the system, the ''brain surface-cerebral fluid space-skull bones'' (BFS).[39] The tester is a cylinder with a movable piston installed inside. The piston's position is adjusted with a micrometer. The device has a special socket where a fragment of human frontal bone and the emitting/sensing module are placed. A schematic representation of the experimental system is shown in Figure 9.

Measurements with and without the 3 mm layer imitating the skin were performed. However, the optical parameters of the skin-imitating layer in the prototype model proved too poor an approximation of those of the live skin and therefore the experiments described in this study were performed on a simplified model of ''***brain–cerebrospinal fluid-skull***'' system [BFS]. In the initial experiments, however, we have noticed that the skin-imitating layer did NOT affect the magnitude of relative changes in received power as a function of SAS width at source-detector distances exceeding 8 mm, i.e., at distances of greatest interest to us. Simultaneously, we did observe a significant attenuating influence of the skin-imitating layer on the absolute power of the received signal, i.e., the absolute power of signal was significantly higher in the model without this layer.

In the search for the best imitation of the surface of the brain we tested a number of substances of varied reflectance ratios. In the particular case of the mechanical-optical model, it should ideally possess the same values of coefficients of absorption, diffusion and anisotropy of diffusion as the brain. These parameters determine the reflection coefficient and depth of penetration of the medium by light. In our model, the surface of the brain cortex-imitating layer formed the boundary for the fluid layer. When the length of this fluid layer is much greater than the penetration depth of the neighboring tissue layers, the optical transmission properties of the fluid layer depend predominantly on its width (thickness) and reflection coefficient. The depth of brain tissue penetration by NIR light is equal to 2.1 mm. This is why reflection was the

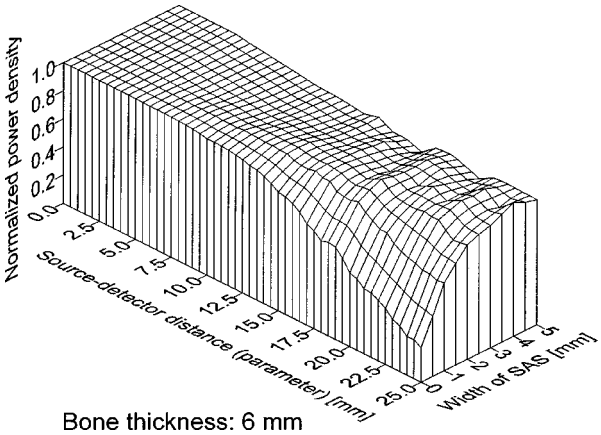

Fig. 6 Relative changes in received power density vs the width of SAS for a given source-detector distance (100 million photons).

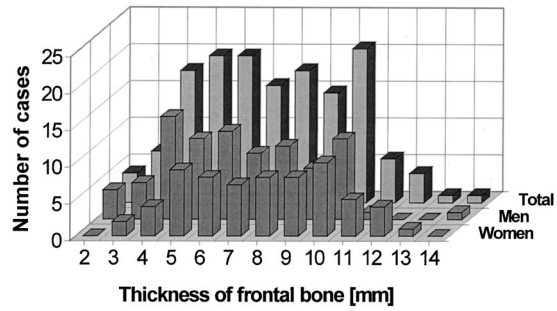

Fig. 7 Distribution of thickness of the frontal bones in 150 human cadavers (measurement taken at the frontal tubers).

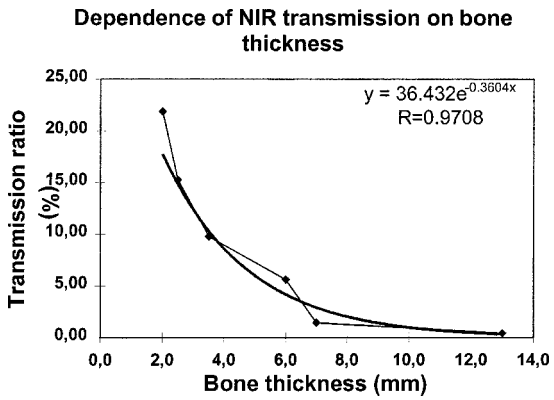

Fig. 8 Transmission of NIR through skull bones of different thickness. Exponential curve $y=36.432e^{-0.3604x}$ (where x is bone thickness in mm, y is transmission ratio in percent) closely matches the relation between experimental data of transmission ratio and bone thickness (correlation ratio equals $R=0.9708$).

most important phenomenon analyzed in our mechanical-optical model. Of the materials available, the authors chose duracryl No. 4.5 (a special plastic produced by Spofa Dental, Czech Republic) as possessing a reflection coefficient most similar to that of the brain cortex. Therefore the surface of the metal piston of the tester was covered with duracryl. The penetration depth is also much smaller than the width of the fluid space in the case of duracryl coating used in mechanical-optical model.

The space between the fragment of skull bone and the surface of the brain phantom was filled with 0.9% saline imitating the cerebrospinal fluid. This space communicated with an overflow compensation reservoir, which enabled the simulation of fluid redistribution to the fluid space of the spinal cord. The source of radiation was placed on the surface of the bone fragment in fixed position. The width of the space was changed in the range from 0 to 5 mm (in increments of 0.25 mm) with a micrometer.

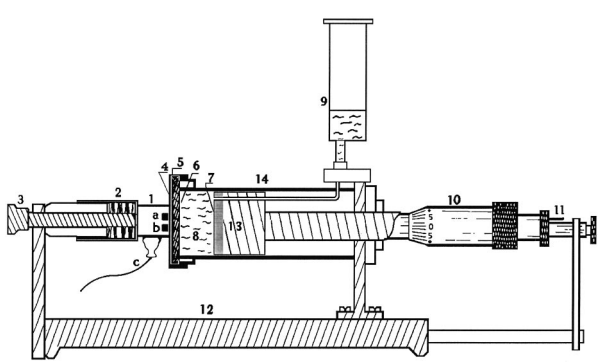

Fig. 9 A schematic representation of the model of the BFS system (modified from Ref. 39). 1-NIR emitting/sensing module A: source, B: detector, C: preamplifier; 2-compression spring; 3-stabilizing unit; 4-plastic film imitating skin; 5-fragment of human frontal bone; 6-thin layer of soft plastic imitating the dura mater of the brain; 7-face of piston covered with 1 cm duracryl layer (imitating the surface of the brain); 8-0.0% saline; 9-compensatory reservoir (overflow safety tank); 10-micrometer; 11-piston adjustment limiter; 12-base construction; 13-piston; 14-cylinder.

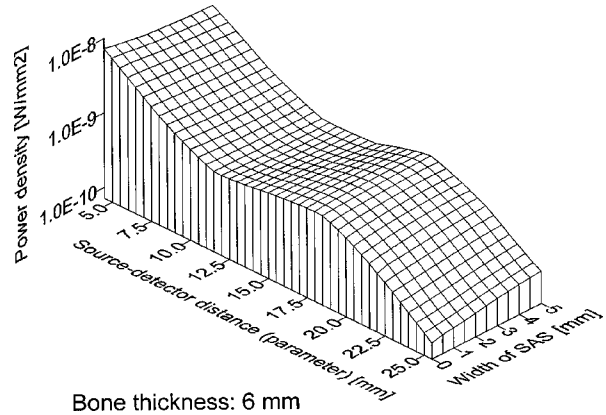

Fig. 10 Measured surface distribution of received power density vs distance from the source and width of SAS.

To assess propagation of radiation in the examined fluid milieu, we performed measurements of reflected power received by the NIR detector. As the source of radiation we used a SFH 484-3 LED ($\lambda=890$ nm, $P=134$ mW, impulse mode). The detector was a photodiode BPW-34. The distance between source and detector was changed within the range 4.5–25.5 mm in increments of 3.5 mm.

The measured distribution of received power density versus distance from the source and width of the SAS and measured relative changes in received power density versus the width of SAS for a given source-detector distance are shown in Figures 10 and 11, respectively.

5 Discussion

The results obtained indicate that it is feasible to assess changes in the width of the SAS with the use of optical radiation. The magnitude of changes in transmission of radiation between the source and detector placed on the surface of the skin of the head, which result from changes in the width of the SAS, is dependent on the source-detector distance. Differences between power densities in Figures 4 and 10 result from the fact that the skin-imitating layer was omitted in the mechanical-optical model due to lack of an appropriate phan-

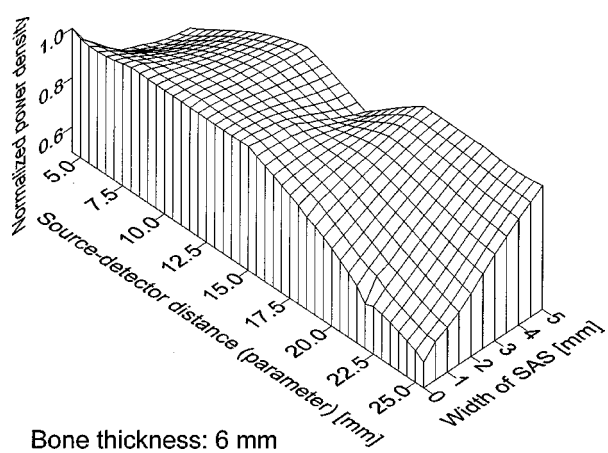

Fig. 11 Measured relative changes in received power density vs the width of SAS for a given source-detector distance.

tom material. Comparison of the two figures indicates that, contrary to the numerical model (Figure 4), in the experiment, a continuous decrease of power with increase in source-detector distance was not observed (Figure 10). This resulted from unevenness of the inner surface of the frontal bone. This is also why the surface plot in Figure 11 is far from flat and exhibits numerous peaks and valleys.

Results presented in Figure 5 indicate that with source-detector distances exceeding 5 mm, the contribution of light propagated in the superficial skin layer to the total signal received by the detector is negligible. Therefore, neglecting the skin-imitating layer in the mechanical-optical model should not affect the relative changes in the signal received by the detector, which are caused by changes in the width of the SAS imitating layer. However, the skin or skin-imitating layer does exert a strong influence on the magnitude of the absolute power of the signal, which is the source of differences between results of the numerical modeling and those from experiment (Figures 4 and 10).

The relations presented in Figures 4 and 5 show, however, that the maximum value of the distance is limited by the minimum power of radiation detectable by the receiving photodiode, i.e., the sensitivity of the detector. For this minimum level of power equal to 1 pW, the maximum source-detector distance is 25 mm. With the detector placed at such a distance from the source, a 1 mm change in the width of the SAS causes a significant change in the power of radiation received, between 10% and 30% (Figures 6 and 11). At source-detector distance lower than a certain value (range 5–20 mm, depending on the thickness of the frontal bone), the amount of radiation propagated to the detector via deep paths in the cerebrospinal fluid is too small in comparison with the very large amount of radiation following the more superficial propagation paths in the skin or skin and bone only. Assessment of the changes in the width of the SAS is then no longer possible. However, placement of the detector in close proximity to the source enables assessment of changes in transmission of radiation in the skin.

The obtained results indicate that the quality and degree of changes in the power of the NIR signal received by the detector, accompanying the changes in SAS width, are dependent on the source-detector distance. When the source-detector distance is short (less than 15 mm—see Figures 6 and 11), the power of the reflected NIR stream is almost constant over the whole analyzed range of bone-brain distances. When detector is placed farther from the source, a stronger influence of the width of the fluid-filled space on the power of the received signal is observed. The greater the SAS width, the greater the power of the received signal. This two-phase relation could be explained with the hypothesis of the ''optical duct effect'' occurring in the space between the bone and brain. The optical duct effect results from the propagation of radiation within the thin SAS layer due to multiple diffuse reflections of numerous individual beams from the inner surfaces of the walls of the optical duct. The wider the SAS, the more radiation reaches the detector at the remote position. Conversely, a decrease in the width of the optical duct results in a decrease in the amount of radiation received by the detector.

This observation leads to the conclusion that, with the detector placed far enough from the source, it should be possible to monitor changes in power of the deep reflected NIR signal, i.e., the one that travels in the propagation duct formed by the SAS. It is important to note the strong correlation between the power of the reflected stream and the bone-brain distance. This conclusion is fully consistent with the assumptions presented by other authors[16–18,30] as well as with the results of numerical modeling. However, the other studies described the effect of source-detector distance on the received signal, with a constant width of SAS, and their results were relevant mostly to oximetric applications of NIR.

As to the selection of the source-detector distance, the results obtained in our study converge with those of Okada and his team.[32] Particularly, both teams found that at source-detector distances less than 5 mm, radiation is transmitted virtually only within the skin layer, and that with distances above 15 mm radiation is transmitted also within SAS and brain cortex.

6 Conclusion

In this study, we examined the influence of changes in the width of the SAS on NIR transmission in the tissues of human head. The main goal here is to experimentally verify and provide background for a totally different technique called NIR-Transillumination (NIR-TI).

The results of our experiments prove the feasibility of noninvasive assessment and monitoring of changes in the width of the SAS *in vivo* by the use of optical radiation. Such a noninvasive technique would be of great clinical importance for diagnostic and prognostic purposes in patients with intracranial pathology affecting this variable, e.g., in cerebral edema. The chances of utilization of such a method in humans will be verified in further experiments. Results of experiments evaluating features of the measurement system are the subject of other publications.

References

1. R. Bright, ''Diseases of the brain and nervous system,'' *Reports of Medical Cases Selected With a View of Illustrating the Symptoms and Cure of Diseases by a Reference to Morbid Anatomy*, Vol. 2, case CCV, Longman Rees, Orme, Brown and Green, and Highley, London (1831).
2. R. C. Banagale, ''History of Transillumination,'' *Pediatric Transillumination*, Steven M. Donn, Lawrence R. Kuhns, Eds., Chap. 1, pp. 3–14, Year Book Medical Publishers, Chicago-London (1983).
3. F. F. Jöbsis, ''Non-invasive, infrared monitoring of cerebral and myocardial oxygen sufficiency and circulatory parameters,'' *Science* **198**, 1264–1267 (1977).
4. J. Wyatt, ''Non-invasive brain monitoring with near infrared spectroscopy,'' *Intensive Critical Care Digest* **8**(3), 47–48 (1989).
5. W. N. J. M. Colier, N. J. C. W. van Haaren, M. J. T. van de Ven, H. T. M. Folgering, and B. Oeseburg, ''Age dependency of cerebral oxygenation assessed with near infrared spectroscopy,'' *J. Biomed. Opt.* **2**(2), 162–170 (1997).
6. J. S. Brazy, D. V. Lewis, M. H. Mitnick, and F. F. Jöbsis van der Vliet, ''Noninvasive monitoring of cerebral oxygenation in pre-term infants: Preliminary observations,'' *Pediatrics* **75**(1), 217–225 (1985).
7. J. S. Wyatt, M. Cope, and D. T. Delpy, ''Quantification of cerebral oxygenation and hemodynamics in sick newborn infants by near infrared spectrophotometry,'' *Lancet* **2**, 1963–1966 (1986).
8. S. Wray, M. Cope, D. T. Delpy, J. S. Wyatt, and E. O. R. Reynolds: ''Characterization of the near infrared absorption spectra of cytochrome aa_3 and hemoglobin for non-invasive monitoring of cerebral oxygenation,'' *Biochim. Biophys. Acta* **933**, 184–192 (1988).
9. J. S. Wyatt, M. Cope, and D. T. Delpy, ''Responses of cerebral vasculature to changes in arterial carbon dioxide tension measured by

near infrared spectroscopy in newborn infants,'' *Pediatr. Res.* **22**, 230 (1988).
10. P. W. McCormick, M. Stewart, M. Dujovny, and J. I. Ausman, ''Clinical application of diffuse near infrared transmission spectroscopy to measure cerebral oxygen metabolism,'' *Hospimedica* **VIII**(4), 39–47 (1990).
11. P. W. McCormick, M. Stewart, M. G. Goetting, M. Dujovny, G. Lewis, and J. I. Ausman, ''Noninvasive cerebral optical spectroscopy for monitoring cerebral oxygen delivery and hemodynamics,'' *Crit. Care Med.* **19**(1), 89–97 (1991).
12. P. Rolfe, Y. A. B. D. Wickramasinghe, and M. Thorniley, ''The potential of near infrared spectroscopy for detection of fetal cerebral hypoxia,'' *Eur. J. Obstet. Gynecol. Reprod. Biol.* **42**, 24–28 (1991).
13. P. H. Klose, G. D. Lewis, W. P. Messing, R. R. Kasperski, and J. M. Flemming, ''Non-invasive infrared cerebral oximetry,'' *Proc. SPIE* **1641**, 202–207 (1992).
14. P. M. S. O'Brien, P. M. Doyle, and P. Rolfe, ''Near infrared spectroscopy in fetal monitoring,'' *Br. J. Hosp. Med.* **49**, 493–487 (1993).
15. M. Firbank, M. Schweiger, and D. T. Delpy: ''Investigation of light piping through clear regions of scattering,'' *Proc. SPIE* **2389**, 167–173 (1996).
16. M. Firbank, S. R. Arridge, M. Schweiger, and D. T. Delpy: ''An investigation of light transport through scattering bodies with non-scattering regions,'' *Phys. Med. Biol.* **41**, 767–783 (1996).
17. E. Okada, M. Saito, M. Firbank, and D. T. Delphy, ''Monte Carlo investigation of the effect of skull optical properties on optical path-length in the brain,'' *Proc. SPIE* **3194**, 28–33 (1997).
18. P. J. Kirkpatrick, ''Use of near-infrared spectroscopy in the adult,'' *Philos. Trans. R. Soc. Lond. B Biol. Sci.* **352**, 701–705 (1997).
19. L. G. Henyey and J. L. Greenstein, ''Diffuse radiation in the galaxy,'' *Astrophys. J.* **93**, 70–83 (1941).
20. R. Marchesini, A. Bertoni, S. Andreola, E. Melloni, and A. E. Sichirollo, ''Extinction and absorption coefficients and scattering phase functions of human tissues in vitro,'' *Appl. Opt.* **28**(12), 2318 (1989).
21. W. F. Cheong, S. A. Prahl, and A. J. Welch, ''A review of the optical properties of biological tissues,'' *IEEE J. Quantum Electron.* **26**(12), 2166 (1990).
22. M. S. Patterson, B. C. Wilson, and D. R. Wyman, ''The propagation of optical radiation in tissue. 1. Models of radiation transport and their application,'' *Laser Med. Sci.* **6**, 155 (1991).
23. M. S. Patterson, B. C. Wilson, and D. R. Wyman, ''The propagation of optical radiation in tissue. 2. Optical properties of tissue and resulting fluency distributions,'' *Laser Med. Sci.* **6**, 379 (1991).
24. A. Ishimaru, *Wave Propagation and Scattering in Random Media*, Vol. 1, Academic Press, New York (1978).
25. J. Haselgrove, J. Leigh, C. Yee, W. Nai-Guang, M. Maris, and B. Chence, ''Monte Carlo and diffusion calculations of photon migration in noninfinite highly scattering media,'' *Proc. SPIE* **1431**, 30–41 (1991).
26. S. Jacques, A. Gutsche, J. Schwartz, L. Wang, and F. Tittel, ''Video reflectometry to specify optical properties of tissue *in vivo*,'' in *Medical Optical Tomography: Functional Imaging and Monitoring*, G. Müller, B. Chance, R. Alfano, S. Arridge, J. Beuthan, E. Gratton, M. Kaschke, B. Masters, S. Svanberg, and P. van der Zee (Invited book chapter), Eds., pp. 211–226, SPIE Optical Engineering Press, Bellingham, WA (1993).
27. I. M. Sobol, *A Primer for the Monte Carlo Method: A Practical Introduction to the Monte Carlo Method*, CRC Press LLC, N.W. Boca Raton (1994).
28. D. E. Knuth, *Semi-numerical Algorithms: The Art of Computer Programming*, 2nd ed., Vol. 2, Secs. 3.2–3.3, Addison–Wesley, Reading, MA (1981).
29. W. H. Press, B. P. Flannery, S. A. Teukolsky, and W. T. Vetterling, *Numerical Recipes in C: The Art of Scientific Computing*, pp. 212 and 213, Cambridge University Press, New York (1990).
30. E. Okada, M. Firbank, M. Schweiger, S. R. Arridge, M. Cope, and D. T. Delpy, ''Theoretical and experimental investigation of near-infrared light propagation in a model of the adult head,'' *Appl. Opt.* **36**(1), 21–31 (1997).
31. C. R. Simpson, M. Kohl, M. Essenpreis, and M. Cope, ''Near infrared optical properties of ex-vivo human skin and sub-cutaneous tissues measured using the Monte Carlo inversion technique,'' *Phys. Med. Biol.* **43**(9), 2465–2478 (1998).
32. E. Okada, M. Saito, M. Firbank, and D. T. Delphy, ''Monte Carlo investigation of the effect of skull optical properties on optical path-length in the brain,'' *Proc. SPIE* **3194**, 28–33 (1998).
33. S. Wan, R. R. Anderson, and J. A. Parrish, ''Analytical modelling for the optical properties of the skin with *in vitro* and *in vivo* application,'' *Photochem. Photobiol.* **34**, 493–499 (1981).
34. F. Bevilacqua, D. Piguet, P. Marquet, J. D. Gross, B. J. Tromberg, and C. Depeursinge, ''*In vivo* local determination of tissue optical properties: Applications to human brain,'' *Appl. Opt.* **38**(22), 4939–4950 (1999).
35. S. L. Jacques, *Tissue Optics*, Short Course Notes Vol. SC01, SPIE Press, Bellingham (1997).
36. M. Firbank, M. Hiraoka, M. Essenpreis, and D. T. Delpy, ''Measurement of the optical properties of the skull in the wavelength range 650–950 nm,'' *Phys. Med. Biol.* **38**, 503–510 (1993).
37. Z. Skalski, A. Frydrychowski, and R. Mazur, ''Encephalovolumeter IR. Method and instrumentation for assessment of changes in intracranial homeostasis,'' *Bydgoskie Towarzystwo Naukowe*, R. Mazur, Ed., Chap. on cerebral stroke, pp. 181–186, Bydgoszcz Scientific Society, Bydgoszcz (1986).
38. S. L. Jacques, ''The role of skin optics in diagnostic and therapeutic uses of lasers,'' in *Laser in Dermatology*, R. Steiner, Ed., Springer, Berlin (1990).
39. P. van der Zee, M. Essenpreis, and D. T. Delpy, ''Optical properties of brain tissue,'' *Proc. SPIE* **1888**, 454–465 (1993).